AIMS Geosciences

AIMS Geosciences, 12(2): 524–539.
DOI: 10.3934/geosci.2026020
Received: 30 December 2025
Revised: 10 March 2026
Accepted: 16 April 2026
Published: 25 May 2026

https://www.aimspress.com/journal/geosciences

Research article

Mid-Holocene peat formation and environmental context in the Ningshao Plain (Southern Hangzhou Bay), East China

Zhujun Hu[1,2,*], Yue Fang[1], Yunfei Zheng[3] and Chunhai Li[4,*]

[1] School of Geography Science, Nanjing Normal University, Nanjing, 210023, China
[2] Jiangsu Center for Collaborative Innovation in Geographical Information Resource Development and Application, Nanjing Normal University, Nanjing 210023, China
[3] Institute of Environmental Archaeology, Nanjing Normal University, Nanjing 210023, China
[4] State Key Laboratory of Lake Science and Environments, Nanjing Institute of Geography and Limnology, Chinese Academy of Sciences, Nanjing 21008, China

* **Correspondence:** Email: zhujunhu@njnu.edu.cn, chhli@niglas.ac.cn; Tel:+86-15861813658, +86-13814047913.

Abstract: Peatlands play a critical role in global carbon cycling, long-term ecological dynamics, and climate-carbon feedbacks, making their formation processes a key focus of global change research. The Ningshao Plain, a coastal lowland in eastern China, contains extensive Holocene peat deposits that developed mainly between ~7.0 and 2.5 cal ka BP. However, the mechanisms driving peatland formation in this region remain poorly understood. In this study, we present new diatom data from the well-dated T1041 profile at the Tianluoshan site in the Ningshao Plain, integrated with published pollen and carbonized seed records, to investigate the drivers of three mid-Holocene peat-forming episodes at 6.5–6.4, 5.2–5.1, and 4.4–4.3 cal ka BP. These peat layers formed under contrasting hydrological conditions, yet each is overlain by flooding deposits, likely associated with storm surges and/or extreme rainfall. Such event layers introduced substantial clastic materials into the wetlands, resulting in waterlogging and persistent anaerobic conditions conducive to peat accumulation. Our results indicate that peatland deposits in the Ningshao Plain constitute sensitive archives of abrupt hydrological responses to mid-Holocene weak monsoon events.

Keywords: Ningshao Plain; mid-Holocene; peatland formation; hydrological variability; climate change

1. Introduction

Peatlands are among the most important high efficiency carbon sequestration ecosystems over long temporal scales, storing approximately one-third of the world's terrestrial carbon stocks [1–5]. They also constitute a major natural source of methane emissions [6–8]. Therefore, peatlands play a critical role in regulating the global carbon cycle and atmospheric greenhouse gas dynamics [7,9–13]. In recent years, increasing attention has been given to peatland formation processes, long-term ecological dynamics, and their responses to climate changes, making peatlands a central focus of global change research [8,14–17].

Peat formation occurs when net primary productivity exceeds the rate of organic matter decomposition, leading to the accumulation of organic matter and to peat development [18]. Therefore, peat formation and accumulation result from the combined influence of multiple environmental factors, including temperature, precipitation, hydrological conditions, vegetation, and geomorphological conditions [18,19]. Among these factors, climate is generally considered the primary control factor [20]. Roughly 90% of global peatlands are concentrated in the cold temperate and boreal zones of the Northern Hemisphere, where low temperatures and very low evaporation rates promote high effective moisture availability [12,21,22]. Reconstructions based on the global peatland database also indicate that peatland initiation and evolution are strongly controlled by climate change across large spatial and temporal scales [4,23–26]. On the other hand, climate drives changes in hydrological processes and sedimentary environments, associated with changes in water levels and drainage conditions, thereby exerting indirect influence on peatland initiation. For example, in coastal settings, sea-level fluctuations play a critical role [27,28]. In subtropical and tropical regions, peatland development is mostly controlled by sea-level changes and regional hydrological conditions [29].

Peatland research in China began in the 1950s and has since made substantial achievements [30–35]. These studies have deepened our understanding of peat distribution, stratigraphy, carbon storage, and paleoenvironmental evolution across climatic and geomorphological settings. However, researchers have predominantly focused on peatlands of the Qinghai-Tibet Plateau and northeastern China [36–38], where cold climates and permafrost conditions strongly influence peat accumulation and preservation. In contrast, peatland development in coastal subtropical regions has received comparatively limited attention [39,40].

The Ning-Shao Plain, in the coastal region of southeastern China, is a typical coastal lowland formed during the Holocene transgression. Thick peat layers occur widely in this region, covering an area of approximately 250 km², which was primarily developed between 7.0 and 2.5 cal ka BP [41]. Studies indicate that peat formation in this region occurred intermittently during several periods of the Holocene, with peat layers dated to 4.8–4.0 ka BP being particularly widespread [42–44]. In this region, sea-level fluctuations likely represent one of the most important drivers of peat formation during the early Holocene [45], while flood events may also have played a crucial role, especially after 7 ka BP. However, detailed studies addressing these mechanisms remain limited [44]. In this study, we

present new diatom data from the T1041 profile at the Tianluoshan site in the Ningshao Plain. These data are integrated with published high-resolution chronological, pollen, and charred seed data from this profile [42,46,47], as well as with regional records from other studies in Ningshao Plain, to identify the drivers of three mid-Holocene peat formation events.

2. Materials and methods

2.1. Study site

The Ningshao Plain is a low-lying coastal mudflat in the Lower Yangtze Valley of East China (Figure 1). The region experiences pronounced seasonal variations in temperature and precipitation under the influence of the East Asian monsoon. The annual mean temperature is 16.2 °C, and the annual mean precipitation is approximately 1600 mm, with most rainfall occurring in July. This area is highly sensitive to tropical climate variations, such as El Niño–Southern Oscillation (ENSO), which modulates the East Asian monsoon system through complex ocean-atmospheric interactions. Regional vegetation is characterized by subtropical mixed forests composed of evergreen and deciduous trees, mostly including *Lithocarpus*, *Cyclobalanopsis*, *Quercus*, *Liquidambar*, *Castanea*, *Aphananthe*, *Celtis*, and *Ulmus*.

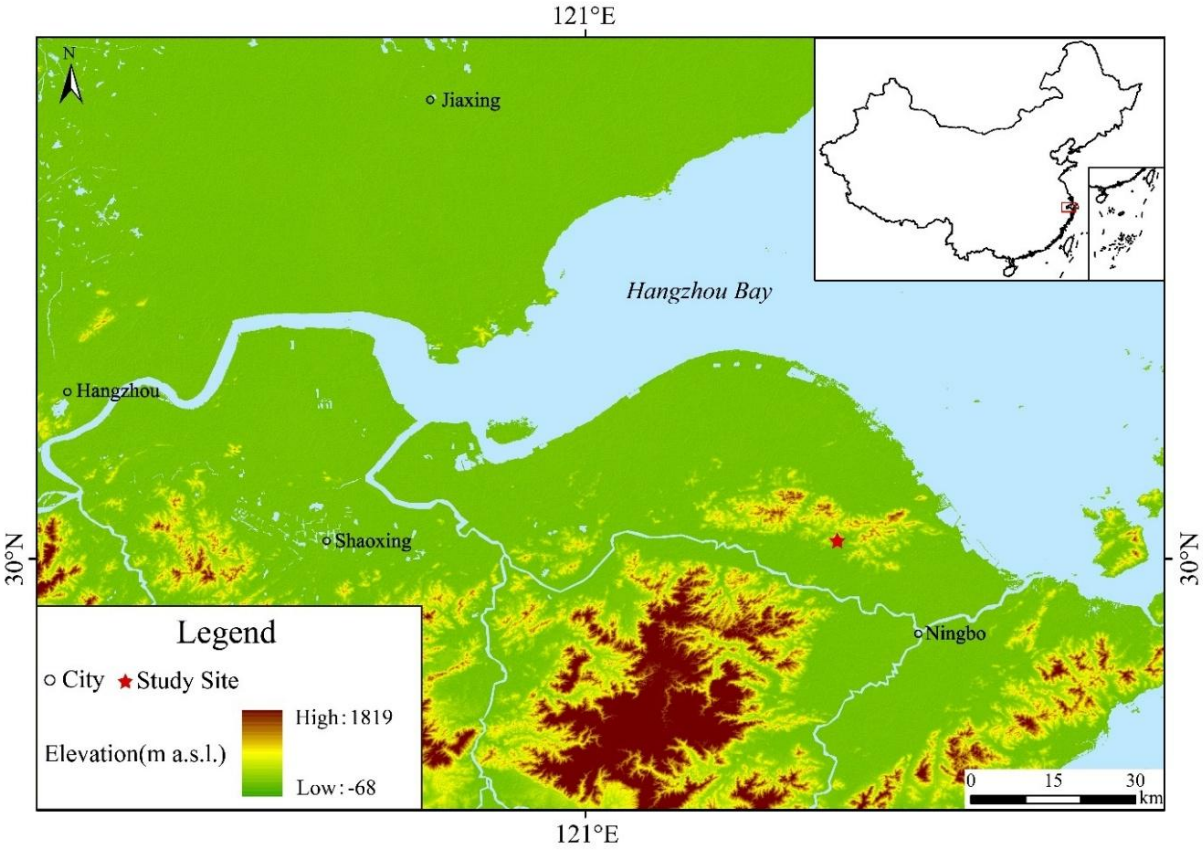

Figure 1. Location of the T1041 profile at the Tianluoshan site.

The Tianluoshan site is at the center of a small basin surrounded by several low mountains on the northeastern flank of the Ningshao Plain, south of the Hangzhou Bay (Figure 1). The site is at an

elevation of 1.83 m above sea level. Evidence from charcoal, phytoliths, carbonized seeds, and other plant macrofossils data in profiles T1041 and T705 indicate the presence of paddy fields at depths of 300–210 cm and 200–100 cm, corresponding to the early and late Hemudu cultural phases, respectively [46]. These findings suggest long-term human modification of the local wetland environment and highlight the close interaction between early rice agriculture, hydrological conditions, and landscape evolution in this coastal lowland setting.

2.2. Methods

2.2.1. Sediment sample

Sediment samples were collected from Trench 1041 (30° 01.355′ N, 121° 22.648′ E) at the Tianluoshan site (Figure 1). This trench exposes a typical stratigraphic sequence with a total thickness of 245 cm. Samples were taken continuously along the north wall of this open profile at 5 cm intervals between 56 and 245 cm, yielding a total of 35 samples.

2.2.2. Chronology

Table 1. AMS 14C dates from the T1041 profile at the Tianluoshan site.

Laboratory no.	Depth (cm)	Materials Dated	Radiocarbon age (^{14}C yr BP)	Calibrated age (cal a BP)			Source
				Mean-age	±2σ	2σ range	
Poz70204	65–70	Plant remains	3840 ± 50	4275	130	4411–4144	[47]
BA398102	70–75	Plant remains	3970 ± 30	4460	65	4523–4396	[47]
Poz66934	70–75	Seeds	3810 ± 70	4240	170	4413–4069	[47]
Poz69037	75–80	Plant remains	4000 ± 70	4445	200	4649–4243	[47]
Poz69036	75–80	Seeds	3890 ± 35	4325	90	4417–4232	[47]
BA398100	75–80	Seeds	3830 ± 30	4225	80	4303–4147	[47]
BA07762	81–86	Plant remains	3760 ± 40	4150	90	4241–4058	[42]
BA07761	96–101	Yagara bulrush	4015 ± 45	4510	105	4621–4403	[42]
BA07760	106–111	Bulrush	4195 ± 70	4695	170	4861–4526	[42]
BA08203	121–126	Bulrush	4470 ± 45	5130	170	5303–4960	[42]
BA07758	131–136	Yagara bulrush	4765 ± 35	5520	60	5587–5459	[42]
BA08895	136–141	Yagara bulrush	4830 ± 35	5540	60	5601–5476	[42]
BA08894	141–146	Yagara bulrush	4965 ± 35	5670	70	5749–5597	[42]
BA08893	146–151	Yagara bulrush	5040 ± 40	5805	100	5902–5705	[42]
BA07764	223–228	Flatdstalk bulrush	5785 ± 60	6565	120	6685–6444	[42]
BA07763	228–233	Flatdstalk bulrush	6045 ± 45	6890	110	7001–6781	[42]

A total of 16 AMS 14C ages were obtained from terrestrial plant remains, consisting of plant fragments that were unidentifiable, and bulrush seeds extracted from this section (Table 1), which were published in Li et al. [47]. In this study, radiocarbon dates were recalibrated using the OxCal 4.4 computer program in conjunction with the IntCal20 calibration dataset [48]. A Bayesian age–depth model was constructed using the R software package Bacon [49].

2.2.3. Total organic carbon (TOC) analyses

Sediment samples were pre-treated with 10% HCl to remove carbonates prior to analysis. Total organic carbon content (TOC) was measured using an EA3000 Elemental Analyzer in Nanjing Institute of Geography and Limnology, Chinese Academy of Sciences. Replicate analyses of homogenized samples indicated an analytical precision better than ±0.1% (1 SD, 1 standard deviation).

2.2.4. Diatom, pollen, and seed analyses

A total of 35 samples were analyzed for diatoms. Diatom slides were prepared following standard laboratory procedures [50]. Samples were treated with 30% H_2O_2 and 10% HCl to remove organic matter and carbonates, respectively, and diatom concentrations were estimated using the microsphere method [51]. Two flotations were performed using a heavy zinc bromide liquid with a specific gravity of 2.3. Cleaned residues were dried onto coverslips and permanently mounted using Naphrax®.

Diatoms were identified and counted under oil immersion at 1000× magnification using an OLYMPUS BX-51 microscope, with at least 300 valves counted per sample. Taxonomic identification mostly followed Krammer and Lange-Bertalot [52], Guo and Qian [53], and Jin et al. [54,55]. Here, we focused on the ecological background of peat formation; detailed analyses of diatom assemblage changes and their environmental implications will be presented in future work.

Pollens were analyzed at 2 cm intervals within 56–155 cm, and at 5 cm spacing for the depth interval between 155 and 245 cm, while 40 samples were used for seeds (see detailed information in Li et al. [42]; Zheng et al. [47]).

3. Results

3.1. Stratigraphy

Based on lithological characteristics and a TOC threshold of >20%, three peat layers were identified in the T1041 profile (Figure 2). The first peat layer occurs at depths of 210–205 cm, with a TOC content of approximately 20%. The second peat layer is between 126 and 122 cm and has an average TOC content of ~22%. The third peat layer occurs at depths of 92–82 cm and is characterized by the highest organic content, with an average TOC content of ~30%.

All peat layers are embedded within clay-rich sediments, indicating deposition under low-energy, fine-grained sedimentary environments. The interval between 50 and 82 cm consists of brownish-yellow silty clay, which likely reflects relatively higher oxidation conditions or enhanced detrital input. In contrast, sediments from 92–118 cm and 128–205 cm are dominated by light gray silty clay,

suggesting more persistent waterlogged conditions. The basal section between 210 and 250 cm is composed mainly of dark gray silty clay, which is indicative of reduced conditions and limited oxygen availability at the sediment–water interface.

3.2. Chronology

All radiocarbon ages obtained from the T1041 profile at the Tianluoshan site are provided in Table 1, and the corresponding age-depth model is shown in Figure 2. The model shows a generally consistent sedimentation history with no major chronological inversions. According to this model, the first peat layer (210–205 cm) dates to 6530–6470 cal a BP, the second peat layer (126–122 cm) to 5240–5120 cal a BP, and the third peat layer (88–82 cm) to 4420–4350 cal a BP, indicating episodic peat formation during the mid-Holocene.

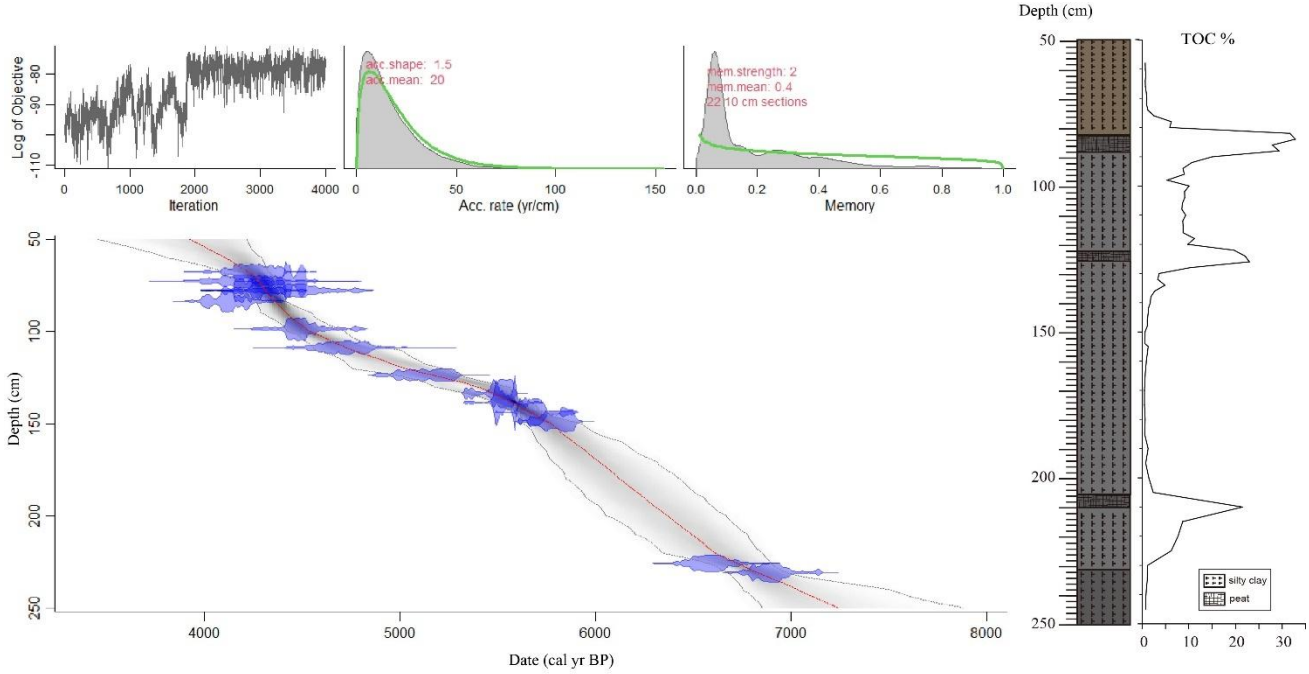

Figure 2. Age-depth model, lithology, and TOC content of the T1041 profile at the Tianluoshan site.

3.3. Diatoms, pollen, and seeds

A total of 31 genera and 81 diatom species were identified from the 35 samples analyzed. As we focused on broad taxonomic and ecological groups, only the classification results of the diatom assemblages are presented (Figure 3). Based on salinity preferences, the diatom assemblages can be divided into three ecological groups: (1) A marine group, consisting of benthic or epiphytic *Actinoptychus undulatus*, *Actinoptychus splendens*, *Navicula elegan*, *Navicula yarren*, *Nitzschia cocconeiformis*, and T*riceratium favus* f. *favus*; (2) a brackish group, mostly consisting of planktonic *Cyclotella meneghiniana*, benthic or epiphytic *Campylodiscus clypeus*, *Campylodiscus echeneis*, *Cyclotella stylorum*, *Cyclotella striata*, *Diploneis smithii*, and *Nitzschia scalaris*; and (3) a freshwater group, including planktonic *Aulacoseira crenulata*, benthic or epiphytic *Cymbella aspera*, *Pinnularia*

spp (*Pinnularia interrupta*, *Pinnularia gibba*, *Pinnularia major*, *Pinnularia virids*), and small *Fragilaria* (*Fragilaria brevistriata and Fragilaria construens* vars. *construens*).

Selected pollen data include the relative abundance of drought-tolerant *Artemisia*, wetland types *Cyperaceae* and *Typha*, and Poaceae >38μm, which mainly indicates the *Oryza*-type Poaceae pollen. *Cyperus* + *Scirpus planiculmis* from seed data are also associated with wetland conditions.

In the first peat layer (210–205 cm, 6.5–6.4 cal ka BP), diatom assemblages are dominated by freshwater benthic groups (43%), particularly *Pinnularia* spp. and small *Fragilaria*. This assemblage is accompanied by a substantial proportion of brackish species (33%), which exhibit an upward-increasing trend within the peat layer, including *D. smithii*, *C. meneghiniana*, and *N. scalaris*. Marine taxa are rare or absent. In the overlying layer (205–190 cm), brackish species become dominant (50–71%), while the proportion of marine taxa increases, indicating enhanced saline influence following peat formation. During this period, the pollen data show that the relative abundance of *Cyperaceae* increases, the Poaceae >38 μm decreases, and seed data *Cyperus* + *Scirpus planiculmis* also show a decreasing trend.

The second peat layer (126–122 cm, 5.2–5.1 cal ka BP) exhibits a diatom assemblage broadly similar to that of the first peat layer. Freshwater taxa dominate the assemblage (57–65%), again characterized by *Pinnularia* spp. and small *Fragilaria*. Brackish taxa form an important subdominant component (32–40%), mostly represented by *D. smithii* and *N. scalaris*. In the overlying sediments, the abundance of brackish and marine species increases, accompanied by a corresponding decline in freshwater species. Furthermore, the relative abundance of *Artemisia* reaches a peak of approximately 9%, then declines to low values. *Typha* shows a relatively high abundance (average 38%), while the Poaceae > 38 μm and seed data *Cyperus* + *Scirpus planiculmis* are at low abundance. In the overlying strata of the second peat layer, the content of *Typha* peaks and then declines, while that of *Cyperaceae* remains consistently low. The content of Poaceae > 38 μm experiences a brief decrease before rising rapidly.

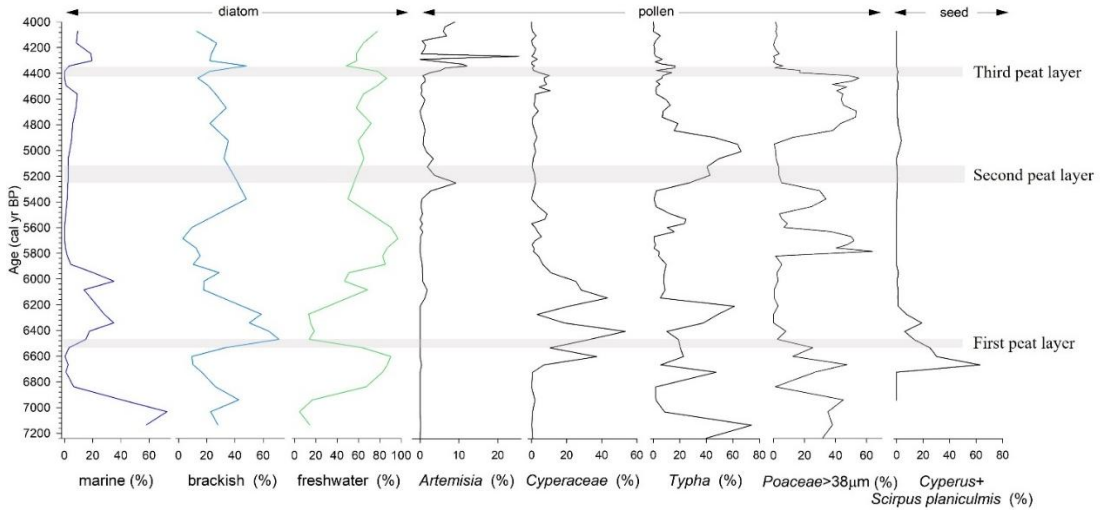

Figure 3. Relative abundance of diatom taxa (marine, brackish, and freshwater), selected pollen data include *Artemisia*, *Cyperaceae*, *Typha*, Poaceae > 38 μm, and *Cyperus* + *Scirpus planiculmis* from seed data.

In the third peat layer (88–82 cm, 4.4–4.3 cal ka BP), diatom assemblages are characterized by markedly higher proportion of freshwater taxa (78–86%) than the first and second peat layer. Dominant taxa include *Pinnularia* spp. and *Navicula* spp. Brackish taxa account for a smaller fraction (14–22%), mainly *D*. *smithii*. The pollen data show that the content of *Artemisia* increases again, coinciding with a decline in Poaceae > 38 μm. In the overlying layer (80–60 cm), the relative abundance of marine and brackish taxa initially increases and then decreases upward, indicating a transient enhancement of saline influence following peat deposition, while the relative abundance of *Artemisia* fluctuates upward, reaching 25% at 72 cm, with relatively low content of Poaceae >38 μm.

4. Discussion

4.1. Mid-Holocene wetland environments and regional peat formation patterns

From the early Holocene to 7 cal ka BP, the study area experienced extensive marine transgression. After 7 cal ka BP, due to the slowed rate of sea-level rise and the increased terrestrial sediment inputs, the shoreline retreated eastward [56,57]. However, this area was prone to hydrological disturbances, such as storm surges and floods [58]. Significant water level fluctuations hindered the long-term stable accumulation of organic matter, which was thus unfavorable for peat development [59]. In addition, substantial sediment inputs from rivers made it difficult for organic matter to accumulate to reach peat formation thresholds under normal conditions [59]. Consequently, peat formation in this region primarily occurs when wetlands encounter sudden hydrological events that create anaerobic conditions favoring vegetation burial and peat formation.

The formation of peat layers in this region was driven by natural processes, independent of anthropogenic interference. All three peat layers in the T1041 profile coincide with low abundance of Poaceae > 38μm (Figure 3). Based on diatom, pollen, and seed records from the T1041 profile (Figure 3), freshwater-brackish marshes were the dominant environments around the Tianluoshan site between 7.0 and 4.0 cal ka BP. During this period, the Ningshao Plain was characterized primarily by extensive marshland [41,56], providing a suitable geomorphological and environmental background conducive to the development of Neolithic cultures in the region [57]. Three peat layers were identified in the T1041 profile, dated to 6.5–6.4, 5.2–5.1, and 4.4–4.3 cal ka BP, respectively. Consistent with our findings, studies across the Ningshao Plain indicate that peatlands, since ~7 cal ka BP, mainly formed during three intervals: 6.7–6.2 cal ka BP [43,44,56,60–62], 5.4–5.0 cal ka BP [63], and 4.8–4.0 cal ka BP [44,58,60].

It is noteworthy that there are two peat layers in the T705 profile, which is also at the Tianluoshan site [60]. The lower peat layer is at the depth of 255–280 cm, dated to 6.4 cal ka BP. It can be considered synchronous with the first peat layer in T041 (210–205 cm, 6.5–6.4 cal ka BP) but occurs at different depths; the upper peat layer in T705 is at the depth of 95–80 cm, dated to 4.8 cal ka BP [60]. It closely corresponds to that at the Yushan site (north Ningshao Plain), which is around 4.7 cal ka BP [58]. In contrast, the third peat layer in T1041 (88–82 cm, 4.4–4.3 cal ka BP) developed at a similar depth. This suggests that peat development at different sites was strongly influenced by local microtopography, which controlled sedimentation rates, hydrological conditions, and the preservation of peat layers.

4.2. Formation of the first peat layer related to storm-surge forcing

The first peat layer at 6.5–6.4 cal ka BP in the T1041 profile (Figure 3) is characterized by diatom assemblages dominated by freshwater taxa, indicating the development of a freshwater marsh environment. Consistently, pollen and seed records show that local vegetation was dominated by wetland types, particularly *Cyperus* and *Typha* (Figure 3), supporting a freshwater wetland setting.

In contrast, the sediments overlying this peat layer are dominated by brackish diatom assemblages (Figure 3). Pollen data indicate a pronounced increase in *Typha*, while seed assemblages are also characterized by the predominance of wetland indicator sedges (*Cyperus* spp.), reflecting the transition from a freshwater wetland to a brackish intertidal wetland under increased saline influence. The development of the first peat layer is linked to abrupt hydro-climatic events, characterized by a period of intensified fluvial activity and flooding. Studies from the Ningshao Plain also document paleostorm surge events during ~6.5–6.3 cal ka BP, evidenced by the occurrence of dinoflagellates in the HMD core [61], brackish diatoms in the HMD1401 core [64], the presence of foraminifera and dinoflagellates in the YJ1506 core [56], the dominance of brackish diatoms [60],and pronounced $\delta^{13}C$ and δD excursions [65] in the Tianluoshan T705 profile. Additional evidence, such as the elevated Sr/Ba ratios and Ca contents at the Wuguishan site, to the east of the Ning-Shao Plain [66], and dinoflagellates in the Loujiaqiao site [67] further imply episodic marine incursions affecting a wide area of the Ningshao Plain and the adjacent Hangzhou Bay region. Such an event was likely linked to the 6.3 ka climate event, which elevated groundwater levels and promoted prolonged waterlogging, thereby creating favorable conditions for peat formation. Consequently, the development of the first peat layer in the Tianluoshan T1041 can be interpreted as a response to storm-surge forcing superimposed on a high water level coastal setting.

4.3. Combined effects of salinity intrusion and flooding on the formation of the second peat layer

The pollen assemblage of the second peat layer at 5.2–5.1 cal ka BP in the Tianluoshan T1041 profile is characterized by a high proportion of *Artemisia*, suggesting relatively dry climatic conditions (Figure 3). Moreover, the diatom assemblage is dominated by brackish taxa. The dry condition may have facilitated seawater intrusion by reducing fluvial discharge and sediment supplies while promoting the development of shallow marsh environments favorable for peat accumulation. In the overlying sediments, a pronounced increase in wetland *Typha*, accompanied by a marked decline in *Artemisia* (Figure 3), indicates a rapid rise in water levels or expanded water area. Diatom records show a sharp decrease in brackish taxa and a corresponding increase in freshwater species (Figure 3), suggesting a transition from a brackish shallow marsh to an inundated freshwater wetland.

Studies suggest that, under the influence of mid-Holocene climate variability, the Ningshao Plain experienced a series of intensified hydrological events with strong spatial and temporal heterogeneity, resulting in asynchronous environmental responses across the region. There is evidence for saline intrusion and flooding between ~5.4 and 5.0 cal ka BP from the Neolithic sites in Ningshao Plain, including Hukengji [68], Xiawangdu [69], Yushan [58], Yingjia [70], Jingtou Mountain [71], and Hemudu [61] sites, and the T705 profile at Tianluoshan site [60]. In addition, intensified precipitation

and flooding during this interval are also documented in Ningshao Plain, such as at Hukengji [68] and Xiawangdu [69] archaeological sites, the Shanglin Lake core [72], and the YJ1503 core [56].

In contrast, contemporaneous peat deposits in the Taihu region were predominantly formed under freshwater conditions [73]. Similarly, multiple cores along the northern margin of the Yangtze River Delta contain peat layers dated to ~5.6–5.4 cal ka BP but lack foraminifera, suggesting deposition in coastal freshwater marsh environments rather than under direct marine influence [45]. This spatial heterogeneity indicates that peatland development across the Ningshao Plain and the Yangtze River Delta between ~5.4 and 5.0 cal ka BP was controlled by the combined effects of storm surge and episodic flooding, modulated by local geomorphological and hydrological conditions. These hydrological extremes were likely associated with the 5.2 ka climatic event, reflecting a regional manifestation of broader-scale global climate variability.

4.4. Formation and burial of the third peat layer and the 4.2 ka event

The third peat layer at 4.4–4.3 cal ka BP in the T1041 profile is widely distributed across the Ningshao Plain. This peat layer is characterized by freshwater diatom group dominance, while pollen records show a trend of increasing abundance of *Artemisia*. This indicates the development of a freshwater marsh under relatively arid climatic conditions.

This peat layer is overlain by brownish-yellow silty clay (Figure 3), with increased abundance of brackish and marine diatom species. The silty clay atop this peat layer reflects a high-energy hydrological event, likely associated with enhanced flooding or marine incursions. Similar stratigraphic patterns have been reported at the Yushan site [58] and in the T705 profile at Tianluoshan site [60]. Evidence from the Shi'ao site further indicates that peat dated to 4.3–4.0 cal ka BP occurs widely across the Ningshao Plain [44]. Studies document pronounced rapid climate fluctuations during this interval, particularly the 4.2 ka event, characterized by rapid El Niño-like and La Niña-like oscillations [47,74]. Peat formation and its subsequent burial during this event was therefore likely driven by extreme hydrological events in response to abrupt climatic changes.

The formation of the three peat layers in T1041 profile coincided with mid-Holocene climate events at ~6.3, 5.2, and 4.2 ka, respectively. These hemispheric-scale events triggered a weakening of the Asian summer monsoon, leading to a "north-dry/south-wet" hydroclimatic pattern in China [75,76]. Studies suggest that weak monsoon periods in the Yangtze River Delta were marked by elevated flood frequency and intensified typhoon activity [72]. Our results, supported by other records from the Ning-Shao Plain, indicate that peat formation is closely associated with floods and storm surges, thereby acting as a regional indicator of mid-Holocene weak monsoon events.

5. Conclusions

Based on multiproxy records from the T1041 profile and regional records, the hydrological conditions associated with the development of the three peat layers were not the same. The first peat layer was formed under relatively humid conditions, whereas the second and third peat layers were developed under comparatively drier conditions. All peat layers are commonly overlain by silty clay that was deposited rapidly during storm surges or flood events, along with less developed rice

cultivation, based on the diatom, selected pollen, and seed records. Such rapid burial of marsh reflects high-energy hydrological conditions, which are critical for maintaining anoxic environments conducive to peat preservation.

Regional evidence from the Ningshao Plain further indicates that all three peat-forming intervals coincided with episodes of enhanced storm-surge activity. Intensified precipitation and flooding during these events raised wetland water levels, promoting prolonged waterlogging and the formation of anaerobic conditions. Increased water availability favored the growth of aquatic vegetation, and its subsequent decay under anoxic conditions contributed substantially to peat accumulation. In addition, erosion and sediment transport associated with intensified storm surges and flood events delivered large volumes of clastic materials into wetland environments, which quickly buried the aquatic plants, further enhancing anaerobic conditions. Consequently, peat deposits in the Ningshao Plain represent sensitive archives of abrupt hydrological responses to rapid climate change events.

Author contributions

Zhujun Hu designed the study, performed the diatom counting, and wrote the original draft; Chunhai Li contributed to study design and participated in reviewing and editing the manuscript; Yunfei Zheng and Yue Fang contributed to reviewing and editing the manuscript.

Use of AI tools declaration

The authors declare they have not used Artificial Intelligence (AI) tools in the creation of this article.

Acknowledgments

We are grateful to the English revision and helpful comments done by Pro. Yu Shiyoung and Li Yongxiang. We would also like to thank the three anonymous reviewers for their constructive comments, which significantly improved the manuscript.

Conflict of interest

The authors declare no conflict of interest.

References

1. Shurpali NJ, Verma SB, Kim J, et al. (1995) Carbon dioxide exchange in a peatland ecosystem. *J Geophys Res: Atmos* 100: 14319–14326. https://doi.org/10.1029/95JD01227
2. Roulet NT (2000) Peatlands, carbon storage, greenhouse gases, and the Kyoto Protocol: Prospects and significance for Canada. *Wetlands* 20: 605–615. https://doi.org/10.1672/0277-5212(2000)020[0605:PCSGGA]2.0.CO;2

3. Belyea LR, Malmer N (2004) Carbon sequestration in peatland: patterns and mechanisms of response to climate change. *Global Change Biol* 10: 1043–1052. https://doi.org/10.1111/j.1529-8817.2003.00783.x
4. Jahn M, Sachs T, Mansfeldt T, et al. (2010) Global climate change and its impacts on the terrestrial Arctic carbon cycle with special regards to ecosystem components and the greenhouse-gas balance. *J Plant Nutr Soil Sci* 173: 627–643. https://doi.org/10.1002/jpln.200900331
5. Gorham E, Lehman C, Dyke A, et al. (2012) Long-term carbon sequestration in North American peatlands. *Quat Sci Rev* 58: 77–82. https://doi.org/10.1016/j.quascirev.2012.09.018
6. Harriss R, Gorham E, Sebacher D, et al. (1985) Methane flux from northern peatlands. *Nature* 315: 652–654. https://doi.org/10.1038/315652a0
7. Smith LC, MacDonald GM, Velichko AA, et al. (2004) Siberian peatlands a net carbon sink and global methane source since the early Holocene. *Science* 303: 353–356. https://doi.org/10.1126/science.1090553
8. Charman DJ, Beilman DW, Blaauw M, et al. (2013) Climate-related changes in peatland carbon accumulation during the last millennium. *Biogeosciences* 10: 929–944. https://doi.org/10.5194/bg-10-929-2013
9. Gorham E (1991) Northern peatlands: role in the carbon cycle and probable responses to climatic warming. *Ecol Appl* 1: 182–195. https://doi.org/10.2307/1941811
10. MacDonald GM, Beilman DW, Kremenetski KV, et al. (2006) Rapid early development of circumarctic peatlands and atmospheric CH_4 and CO_2 variations. *Science* 314: 285–288. https://doi.org/10.1126/science.1131722
11. Jones MC, Yu Z (2010) Rapid deglacial and early Holocene expansion of peatlands in Alaska. *Proc Natl Acad Sci USA* 107: 7347–7352. https://doi.org/10.1073/pnas.0911387107
12. Yu Z, Beilman DW, Jones MC (2009) Sensitivity of northern peatland carbon dynamics to Holocene climate change. *Carbon Cycling in Northern Peatlands,* 184: 55–69. https://doi.org/10.1029/2008GM000822
13. Yu Z, Beilman DW, Frolking S, et al. (2011) Peatlands and their role in the global carbon cycle. *Eos Trans AGU* 92: 97–98. https://doi.org/10.1029/2011EO120001
14. Clymo RS (1984) The limits to peat bog growth. *Philos Trans R Soc Lond B Biol Sci* 303: 605–654. https://doi.org/10.1098/rstb.1984.0002
15. Belyea LR, Baird AJ (2006) Beyond "the limits to peat bog growth": Cross-scale feedback in peatland development. *Ecol Monogr* 76: 299–322. https://doi.org/10.1890/0012-9615(2006)076[0299:BTLTPB]2.0.CO;2
16. Loisel J, Gallego-Sala AV, Amesbury MJ, et al. (2021) Expert assessment of future vulnerability of the global peatland carbon sink. *Nat Clim Chang* 11: 70–77. https://doi.org/10.1038/s41558-020-00944-0
17. Mander Ü, Espenberg M, Melling L, et al. (2024) Peatland restoration pathways to mitigate greenhouse gas emissions and retain peat carbon. *Biogeochemistry* 167: 523–543. https://doi.org/10.1007/s10533-023-01103-1
18. Moore PD (1989) The ecology of peat-forming processes: a review. *Int J Coal Geol* 12: 89–103. https://doi.org/10.1016/0166-5162(89)90048-7

19. Takada M, Shimada S, Takahashi H (2016) Tropical peat formation, In: Osaki M, Tsuji N, Eds., *Tropical peatland ecosystems*, Tokyo: Springer Japan, 127–135. https://doi.org/10.1007/978-4-431-55681-7_8
20. Heathwaite AL (1993) Disappearing peat-regenerating peat? The impact of climate change on British peatlands. *Geogr J* 159: 203–208. https://doi.org/10.2307/3451411
21. Joosten H, Clarke D (2002) Wise Use of Mires and Peatlands, International Mire Conservation Group and International Peat Society, Saarijärvi, 1–304.
22. Wang Y, Roulet NT, Frolking S, et al. (2009) The importance of northern peatlands in global carbon systems during the Holocene. *Clim Past* 5: 683–693. https://doi.org/10.5194/cp-5-683-2009
23. Ovenden L (1990) Peat accumulation in northern wetlands. *Quat Res* 33: 377–386. https://doi.org/10.1016/0033-5894(90)90063-Q
24. Moore PD (2002) The future of cool temperate bogs. *Environ Conserv* 29: 3–20. https://doi.org/10.1017/S0376892902000024
25. Maltby E (2010) Effects of climate change on the societal benefits of UK upland peat ecosystems: applying the ecosystem approach. *Clim Res* 45: 249–259. https://doi.org/10.3354/cr00893
26. Ruppel M, Väliranta M, Virtanen T, et al. (2013) Postglacial spatiotemporal peatland initiation and lateral expansion dynamics in North America and northern Europe. *Holocene* 23: 1596–1606. https://doi.org/10.1177/0959683613499053
27. Magnan G, Garneau M, Payette S (2014) Holocene development of maritime ombrotrophic peatlands of the St. Lawrence North Shore in eastern Canada. *Quat Res* 82: 96–106. https://doi.org/10.1016/j.yqres.2014.04.016
28. Kreuzburg M, Ibenthal M, Janssen M, et al. (2018) Sub-marine continuation of peat deposits from a coastal peatland in the southern Baltic sea and its Holocene development. *Front Earth Sci* 6: 103. https://doi.org/10.3389/feart.2018.00103
29. Treat CC, Kleinen T, Broothaerts N, et al. (2019) Widespread global peatland establishment and persistence over the last 130,000 y. *Proc Natl Acad Sci USA* 116: 4822–4827. https://doi.org/10.1073/pnas.1813305116
30. Zhao H, Leng X, Wang S (2002) Distribution, Accumulation Rate of Peat in the Changbaishan Mountains and Climate Change in Holocene. *J Mt Sci* 20: 513–518. https://doi.org/10.16089/j.cnki.1008-2786.2002.05.001. In Chinese.
31. Wang G, Liu J, Tang J (2005) Advance in marsh sedimentation and environmental change study. *Adv Earth Sci* 20: 304–311. In Chinese.
32. Zhang Y, Xia D, Zhang Y, et al. (2012) Advances in palaeoclimatic research recorded by peat in China since the last deglaciation. *Adv Earth Sci* 27: 42–51. In Chinese.
33. Xing W, Bao K, Guo W, et al. (2015) Peatland initiation and carbon dynamics in northeast China: links to Holocene climate variability. *Boreas* 44: 575–587. https://doi.org/10.1111/bor.12116
34. Sun J, Li H, Wang J, et al. (2019) Study of Jinchuan Mire in NE China II: Peatland development, carbon accumulation and climate change during the past 1000 years. *Quat Int* 528: 18–29. https://doi.org/10.1016/j.quaint.2019.05.007
35. Zhang P, Zhao C, Huang C, et al. (2023) Soil organic carbon changes in peat bogs on the Qinghai-Tibet Plateau. *Wetlands* 43: 104. https://doi.org/10.1007/s13157-023-01755-7

36. Xu H, Liu B, Lan J, et al. (2013) Holocene peatland development along the eastern margin of the Tibetan Plateau. *Quat Res* 80: 47–54. https://doi.org/10.1016/j.yqres.2013.04.001
37. Zhao Y, Tang Y, Yu Z, et al. (2014) Holocene peatland initiation, lateral expansion, and carbon dynamics in the Zoige Basin of the eastern Tibetan Plateau. *Holocene* 24: 1137–1145.
38. Chen X, McGowan S, Bu Z, et al. (2022) Diatom-inferred microtopography formation in peatlands. *Earth Surf Processes Landforms* 47:672–687. https://doi.org/10.1002/esp.5280
39. Yu M, Tao Y, Liu W, et al. (2020) C, N, and P stoichiometry and their interaction with different plant communities and soils in subtropical riparian wetlands. *Environ Sci Pollut Res* 27: 1024–1034. https://doi.org/10.1007/s11356-019-07004-x
40. Chen C, Huang K, Xie D, et al. (2024) Subalpine peatland development since the Last Glacial Maximum in subtropical China: Predominantly controlled by monsoonal climate and local topography. *Catena* 242: 108084. https://doi.org/10.1016/j.catena.2024.108084
41. Zhang S (1991) The Peat in Ning Shao Plain of Zhe Jiang Province and Its Reflection on The Sea-Level Changes. *J Nanjing Norm Univ (Nat Sci Ed)* 14: 76–84. In Chinese.
42. Li C, Zheng Y, Yu S, et al. (2012) Understanding the ecological background of rice agriculture on the Ningshao Plain during the Neolithic Age: pollen evidence from a buried paddy field at the Tianluoshan cultural site. *Quat Sci Rev* 35: 131–138. https://doi.org/10.1016/j.quascirev.2012.01.007
43. Innes JB, Zong Y (2021) History of mid-and late Holocene palaeofloods in the Yangtze coastal lowlands, east China: evaluation of non-pollen palynomorph evidence, review and synthesis. *Quaternary* 4: 21. https://doi.org/10.3390/quat4030021
44. Wang Y, Song S, Zhang Y, et al. (2023) Brief Report on the Excavation of Ancient Rice Field Remains at the Shiaao Site in Yuyao City, Zhejiang Province. *Archaeology*. In Chinese.
45. Zhan Q, Wang Z (2014) Mid-Holocene sea-level of northern Yangtze River delta reconstructed by salt marsh peat. *J Palaeogeogr* 16: 548–556. In Chinese.
46. Zheng Y, Sun G, Qin L, et al. (2009) Rice fields and modes of rice cultivation between 5000 and 2500 BC in east China. *J Archaeol Sci* 36: 2609–2616. https://doi.org/10.1016/j.jas.2009.09.026
47. Li C, Li Y, Zheng Y, et al. (2018) A high-resolution pollen record from East China reveals large climate variability near the Northgrippian-Meghalayan boundary (around 4200 years ago) exerted societal influence. *Palaeogeogr Palaeoclimatol Palaeoecol* 512: 156–165. https://doi.org/10.1016/j.palaeo.2018.07.031
48. Reimer PJ, Austin Wen, Bard E, et al. (2020) The IntCal20 Northern Hemisphere radiocarbon age calibration curve (0-55 cal kBP). *Radiocarbon* 62: 725–757. https://doi.org/10.1017/RDC.2020.41
49. Blaauw M, Christen JA (2011) Flexible paleoclimate age-depth models using an autoregressive gamma process. *Bayesian Anal* 6: 457–474. https://doi.org/10.1214/11-BA618
50. Battarbee RW, Kneen MJ (1982) The use of electronically counted microspheres in absolute diatom analysis. *Limnol Oceanogr* 27: 184–188. https://doi.org/10.4319/lo.1982.27.1.0184
51. Renberg I (1990) A procedure for preparing large sets of diatom slides from sediment cores. *J Paleolimnol* 4: 87–90. https://doi.org/10.1007/BF00208301
52. Krammer K, Lange-Bertalot H (2012) *European Diatom Identification System*, Sun Yat-sen University Press, Guangzhou, 1–493.

53. Guo Y, Qian S (2003) *Flora Algarum Marimarum Sinicarum: Centricae*, Science Press, Beijing, 1–493. In Chinese.
54. Jin D, Cheng Z, Lin J, et al. (1982) *Chinese Marine Benthic Diatoms,* Vol. I. Beijing: Ocean Press, 1–323. In Chinese.
55. Jin D, Cheng Z, Liu S, et al. (1991) *Chinese Marine Benthic Diatoms,* Vol. II. Beijing: Ocean Press,1-437. In Chinese
56. Liu Y, Sun Q, Fan D, et al. (2018) Early to Middle Holocene sea level fluctuation, coastal progradation and the Neolithic occupation in the Yaojiang Valley of southern Hangzhou Bay, Eastern China. *Quat Sci Rev* 189: 91–104. https://doi.org/10.1016/j.quascirev.2018.04.010
57. Zheng H, Zhou Y, Yang Q, et al. (2018) Spatial and temporal distribution of Neolithic sites in coastal China: Sea level changes, geomorphic evolution and human adaption. *Sci China Earth Sci* 61: 123–133. https://doi.org/10.1007/s11430-017-9121-y
58. Wang Z, Ryves DB, Lei S, et al. (2018) Middle Holocene marine flooding and human response in the south Yangtze coastal plain, East China. *Quat Sci Rev* 187: 80–93. https://doi.org/10.1016/j.quascirev.2018.03.001
59. Clymo RS, Turunen J, Tolonen K (1998) Carbon accumulation in peatland. *Oikos* 81: 368–388. https://doi.org/10.2307/3547057
60. Zheng Y, Sun G, Chen X (2012) Response of rice cultivation to fluctuating sea level during the Mid-Holocene. *Chin Sci Bull* 57: 370–378. https://doi.org/10.1007/s11434-011-4786-3
61. Liu Y, Sun Q, Fan D, et al. (2016) Pollen evidence to interpret the history of rice farming at the Hemudu site on the Ningshao coast, eastern China. *Quat Int* 426: 195–203. https://doi.org/10.1016/j.quaint.2016.05.016
62. Shao K, Lu H, Zhang H (2024) Holocene coastal environmental evolution and human adaptation in the Yaojiang-Ningfeng plain, eastern China, revealed by reanalysis of the radiocarbon dates. *Quat Sci Rev* 327: 108530. https://doi.org/10.1016/j.quascirev.2024.108530
63. Liu Y, Xiao L, Cheng Z, et al. (2023) Anthropogenic impacts on vegetation and biodiversity of the lower Yangtze region during the mid-Holocene. *Quat Sci Rev* 299: 107881. https://doi.org/10.1016/j.quascirev.2022.107881
64. Shao K, Zhang J, Lu H, et al. (2021) Process of rice domestication in relation to Holocene environmental changes in the Ningshao Plain, lower Yangtze. *Geomorphology* 381: 107650. https://doi.org/10.1016/j.geomorph.2021.107650
65. Patalano R, Wang Z, Leng Q, et al. (2015) Hydrological changes facilitated early rice farming in the lower Yangtze River Valley in China: A molecular isotope analysis. *Geology* 43: 639–642. https://doi.org/10.1130/G36783.1
66. Huang J, Lei S, Tang L, et al. (2020) Mid-Holocene environmental change and human response at the Neolithic Wuguishan site in the Ningbo coastal lowland of East China. *Holocene* 30: 1591–1605. https://doi.org/10.1177/0959683620941070
67. Shu J, Jiang L, Cheng Y (2017) Palynological evidence for the formation of the culture interval layers at the Loujiaqiao archaeological site in Zhuji, Zhejiang Province, east China. *Acta Micropalaeontol Sin* 34: 406–417. https://doi.org/10.16087/j.cnki.1000-0674.2017.04.003. In Chinese.

68. Lin F, Mei S, Xu H, et al. (2025) Sedimentary records of mid-Holocene extreme storm events and Neolithic cultural response in the Yaojiang-Ningbo Plain, East China. *Mar Geol* 488: 107611. https://doi.org/10.1016/j.margeo.2025.107611
69. Huang J, Li Y, Ding F, et al. (2021) Sedimentary records of mid-Holocene coastal flooding at a Neolithic site on the southeast plain of Hangzhou Bay, east China. *Mar Geol* 431: 106380. https://doi.org/10.1016/j.margeo.2020.106380
70. Chen Y, Lei S, Lazar M, et al. (2023) Mid-Holocene salinity intrusion and rice yield loss on East China coast and the impacts on formation of a complex state society. *Mar Geol* 466: 107183. https://doi.org/10.1016/j.margeo.2023.107183
71. Pan Y, Sun G, Lei S, et al. (2023) Geochemical characteristics of alkaline earth metals in the sediments of Neolithic sites in the eastern Ningshao Plain and implications for the saltwater intrusion. *Mar Geol Quat Geol* 43: 169–180. https://doi.org/10.16562/j.cnki.0256-1492.2022112202. In Chinese.
72. Yao S, Ling C, Lu H, et al. (2024) Palynological and sedimentological evidence for early mid-Holocene hydroclimatic variability in the Ningshao Plain, East China. *Palaeogeogr Palaeoclimatol Palaeoecol* 637: 111997. https://doi.org/10.1016/j.palaeo.2023.111997
73. Zong Y (2004) Mid-Holocene sea-level highstand along the southeast coast of China. *Quat Int* 117: 55–67. https://doi.org/10.1016/S1040-6182(03)00116-2
74. Zhang H, Cheng H, Sinha A, et al. (2021) Collapse of the Liangzhu and other Neolithic cultures in the lower Yangtze region in response to climate change. *Sci Adv* 7: eabi9275. https://doi.org/10.1126/sciadv.abi9275
75. Wang Y, Cheng H, Edwards RL, et al. (2005) The Holocene Asian monsoon: links to solar changes and North Atlantic climate. *Science* 308: 854–857. https://doi.org/10.1126/science.1106296
76. Zhang H, Cheng H, Cai Y, et al. (2018) Hydroclimatic variations in southeastern China during the 4.2 ka event reflected by stalagmite records. *Clim Past* 14: 1805–1817. https://doi.org/10.5194/cp-14-1805-2018

AIMS Press